

## DROP FORMATION IN CROSS-JUNCTION MICRO-CHANNEL USING LATTICE BOLTZMANN METHOD

by

**Keivan FALLAH<sup>a\*</sup>, Moahammad Taeibi RAHNI<sup>a,b</sup>,  
Alireza MOHAMMADZADEH<sup>a</sup>, and Mohammad NAJAFI<sup>a</sup>**

<sup>a</sup> Department of Mechanical and Aerospace Engineering, Science and Research Branch,  
Islamic Azad University, Tehran, Iran

<sup>b</sup> Department of Aerospace Engineering, Sharif University of Technology, Tehran, Iran

Original scientific paper  
<https://doi.org/10.2298/TSCI160322230F>

*Drop formation in cross-junction micro-channels is numerically studied using the lattice Boltzmann method with pseudo-potential model. To verify the simulation, the results are compared to previous numerical and experimental data. Furthermore, the effects of capillary number, flow rate ratio, contact angle, and viscosity ratio on the flow patterns, drop length, and interval between drops are investigated and highlighted. The results show that the drop forming process has different regimes, namely, jetting, drop, and squeezing regimes. Also, it is shown that increasing in the flow rate ratio in the squeezing regime causes increment in drop length and decrement in drops interval distance. On the other hand, the drops length and the interval between the generated drops increase as contact angle increases. Also, the drop length and distance between drops is solely affected by viscosity ratio.*

**Key words:** *lattice Boltzmann method, pseudo-potential model, drop formation, cross-junction micro-channels*

### Introduction

Over the past two decades, micro-fluidic systems that generate drop/bubble have found numerous applications in cell encapsulation [1], fluorinations [2], drug delivery [3], hydrogenation [4], and so on. Multi-phase flows are very common in micro-fluidic systems. In recent years, a number of numerical and experimental studies have performed to highlight advantage of drop (bubble) generation using a variety of micro-fluidic devices, T-junctions [5-9], cross-junction[10-14], Y-junction[15-17], and so on. Simulation of two-phase flow in complex geometry is a challenging work, because of the inherent difficulty in tracking the fluid interfaces, the correct treatment of the surface tension forces, and mass conservation [18].

Recently, the lattice Boltzmann method (LBM), which is based on mesoscopic kinetic equations, has been proved to be a promising numerically robust technique to simulate complex flows, including natural convection [19], nanofluid [20, 21], non-newtonian [22, 23], unsteady flow [24], and especially two immiscible phases flow in complex geometries. Compared with conventional methods for multi-phase flows, LBM does not track interfaces while sharp interfaces can be maintained automatically [25]. There are several models in the LBM for simulating multi-phase flow including: the free-energy model [26, 27], mean-field model [28, 29], the pseudo-potential model [30, 31] (also known as the Shan-Chen) and other models [32, 33].

\* Corresponding author, e-mail: keyvan.fallah@gmail.com

In this study, the pseudo-potential model has been chosen. The wide applications of this model arise from the following advantages: the programming is very simple, the interface separates automatically, and control of the contact angle and the wetting behavior of the solid phases are easy. The goal of the current study is to investigate the dynamics of the two-phase flow in cross-junction micro-channel. The numerical results are compared to previous numerical and experimental data. The effect of capillary number, flow rate ratio, contact angle and viscosity ratio on the flow patterns, the drop length and distance between drops is investigated.

### Numerical method

In this study, the multi-component LBM with the pseudo-potential model [30, 31] was used for the two-phase flow simulation in micro-fluidic systems. The evolution equation of the lattice Boltzmann equation using the single relaxation time collision for multi-phase flow is [34]:

$$f_i^\sigma(\mathbf{x} + \mathbf{e}_i \delta t, t + \delta t) = f_i^\sigma(\mathbf{x}, t) - \frac{f_i^{\sigma(\text{eq})} - f_i^\sigma}{\tau^\sigma} \quad (1)$$

where  $\delta t$  is the time step size, and  $\sigma$  refers to the component,  $f_i$  – the particle distribution function along the  $i^{\text{th}}$ -direction, and  $f^{\text{eq}}$  – the equilibrium distributions function of  $f$ , and computed:

$$f_i^{\sigma(\text{eq})} = w_i \rho^\sigma \left[ 1 + \frac{\mathbf{e}_i \cdot \mathbf{u}_{\text{eq}}^\sigma}{c_s^2} + \left( \frac{\mathbf{e}_i \cdot \mathbf{u}_{\text{eq}}^\sigma}{2c_s^4} \right)^2 - \frac{\mathbf{u}_{\text{eq}}^\sigma \cdot \mathbf{u}_{\text{eq}}^\sigma}{2c_s^2} \right] \quad (2)$$

where  $\mathbf{e}_i$  denotes the particle velocity in the  $i^{\text{th}}$  direction. Lattice models are usually described as  $D_n Q_m$ , where  $n$  is the dimension and  $m$  – the number of  $i$  directions. In this simulation,  $D_2 Q_9$  is used. Hence, the particle velocity is defined:

$$\mathbf{e}_i = \begin{cases} (0, 0) & i = 0 \\ \left( \cos \left[ \frac{(i-1)\pi}{4} \right], \sin \left[ \frac{(i-1)\pi}{4} \right] \right) c & i = 1, 2, 3, 4 \\ \sqrt{2} \left( \cos \left[ \frac{(i-1)\pi}{4} \right], \sin \left[ \frac{(i-1)\pi}{4} \right] \right) c & i = 5, 6, 7, 8 \end{cases} \quad (3)$$

where  $w_i$  are weighting factors for each velocity ( $w_0 = 4/9$ ,  $w_i = 1/9$  for  $i = 1-4$ , and  $w_i = 1/36$  for  $i = 5-8$ ). The macroscopic density  $\rho$  and velocity  $\mathbf{u}$  in the lattice unit for each component are obtained from:

$$\rho^\sigma = \sum_{i=0}^8 f_i^\sigma, \quad \mathbf{u}^\sigma = \sum_{i=0}^8 \frac{\mathbf{e}_i f_i^\sigma}{\rho^\sigma} \quad (4)$$

The adjusted momentum for each component,  $\mathbf{u}_{\text{eq}}^\sigma$ , appearing in eq. (2) is defined:

$$\mathbf{u}_{\text{eq}}^\sigma = \mathbf{u}' + \frac{\tau^\sigma \mathbf{F}^\sigma}{\rho^\sigma} \quad (5)$$

where  $\tau^\sigma$  is the relaxation time of component  $\sigma$  and is related to kinematic viscosity,  $\mu^\sigma = (\tau^\sigma - 0.5)c_s^2 \delta t$ . Also,  $\mathbf{u}'$  is an effective velocity by the law of total momentum conservation:

$$\mathbf{u}' = \frac{\sum_{\sigma=1}^2 \frac{\rho^\sigma \mathbf{u}^\sigma}{\tau^\sigma}}{\sum_{\sigma=1}^2 \frac{\rho^\sigma}{\tau^\sigma}} \quad (6)$$

where  $\mathbf{F}^\sigma$  is the total interaction force exerted on the  $\sigma^{\text{th}}$  component expressed:

$$\mathbf{F}^\sigma = \mathbf{F}_f^\sigma + \mathbf{F}_s^\sigma + \dots \quad (7)$$

where  $\mathbf{F}_f^\sigma$  and  $\mathbf{F}_s^\sigma$  are the fluid-fluid and the fluid-solid interactive forces, respectively. Based on the original pseudopotential model [31], the fluid-fluid interaction force can be given [35]:

$$\mathbf{F}_f^\sigma = -\psi^\sigma(\mathbf{x}) \sum_{\bar{\sigma}=1}^2 G_{\sigma\bar{\sigma}} \sum_{i=0}^8 w_i \psi_{\bar{k}}(\mathbf{x} + \mathbf{e}_i \delta t) \mathbf{e}_i \quad (8)$$

Here  $G_{\sigma\bar{\sigma}}$  is the interaction strength between the two components  $\sigma$  and  $\bar{\sigma}$ . The  $\psi^\sigma$  is the interparticle potential depending on the local density. In the literature [30, 36, 37], several functional forms of  $\psi^\sigma$  have been proposed. The different choices on  $\psi^\sigma$  will lead to different equations of state. Yuan and Schaefer [37] found that with an appropriate interparticle potential and a proper equation of state, density ratio can be increased with relatively low spurious currents. Hence, we considered the interparticle potential:

$$\psi^\sigma(\mathbf{x}) = \sqrt{\frac{2(P_\sigma - c_s^2 \rho^\sigma)}{G_{\sigma\sigma}}} \quad (9)$$

The Peng-Robinson equation of state used and expressed:

$$P = \frac{\rho RT}{1 - bT} - \frac{a\alpha(T)\rho^2}{1 + 2b\rho - b^2\rho^2} \quad (10)$$

$$\alpha(T) = \left[ 1 + (0.37464 + 1.5422\omega - 0.26992\omega^2)(1 - \sqrt{T/T_c}) \right]^2 \quad (11)$$

where  $a = 0.45724(RT_c)^2/P_c$ ,  $b = 0.0778RT_c/P_c$ . The  $\omega$ ,  $P_c$  and  $T_c$  are acentric factor, the critical pressure, and critical temperature, respectively.

Similarly, the fluid-solid interaction force is calculated by:

$$\mathbf{F}_s^\sigma = -\psi^\sigma(\mathbf{x}) \sum_{i=0}^8 w_i G_{\sigma w} S(\mathbf{x} + \mathbf{e}_i \delta t) \mathbf{e}_i \quad (12)$$

where  $S$  is an indicator function. This is equal to zero for fluid nodes and unit for solid nodes. The  $G_{\sigma w}$  is the interaction strength between solid and fluid component  $\sigma$ . In the pseudo-potential model, wetting conditions on the solid boundary can be easily implemented by relative strength of  $G_{1w}$  and  $G_{2w}$ . When  $G_{1w} - G_{2w} < 0$ , component 1 is modeled as the wetting phase and the component 2 is the non-wetting phase.

### Computational domain and numerical details

Figure 1 shows the schematics of a 2-D cross-junction micro-channel. The micro-channel consists of the main channel with width  $w_c$  and the two lateral channels with the same width

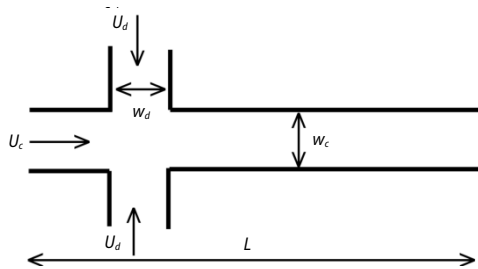


Figure 1. Flow geometry for annulus

The problem can be described by a group of physical parameters: viscosity,  $\mu_c$  and  $\mu_d$ , density,  $\rho_c$ ,  $\rho_d$ , wide of channel,  $w_c$  and  $w_d$ , inlet velocity of phases,  $U_c$  and  $U_d$ , interfacial tension between phases,  $\sigma$ , and contact angle. The subscripts  $c$  and  $d$  represent continuous and dispersed phases, respectively. By using the Buckingham Pi theorem, following non-dimensional numbers are introduced: Reynolds number,  $Re = \rho_c U_c w_c / \mu_c$ , Bond number,  $Bo = \rho_c g w_c^2 / \sigma$ , capillary number,  $Ca = \mu_c U_c / \sigma$ , flow rate ratio,  $Q = U_c w_c / U_d w_d$ , density ratio,  $\rho = \rho_c / \rho_d$ , viscosity ratio,  $\mu = \mu_c / \mu_d$ , and width ratio  $w = w_c / w_d$ . Qian and Lawal [8] and Tice *et al.* [10] argue that inertial and gravity effects are small compared to viscous and interfacial forces in micro-channels. Hence, Reynolds number and Bond number have negligible effects on the formation of drop. Capillary number is the most important parameter to understand flow information in micro-channels and is denoted by capillary number (ratio of viscous to surface tension forces).

### Validation of LBM code

To validate the present study three different cases are considered, *i. e.*, Laplace law, static contact angle and drop formation in cross-junction micro-channel.

#### Laplace law

According to the Laplace law, if the initial shape of the drop is changed from a circle in the 2-D case, in the absence of viscosity and gravity forces, the final shape must be circle due to the pressure difference inside and outside the drop and the surface tension forces. The value of the surface tension is evaluated:

$$\Delta P = \frac{\sigma}{R} \quad (13)$$

where  $\Delta P$  and  $R$  are the pressure jump across the interface and the radius of the drop, respectively.

To verify the Laplace law, initially, a square drop with different length is located in the middle of the computational domain with  $160 \times 160$  lattice units. The periodic boundary condition is used at all boundaries. The pressure jump is plotted against  $1/R$  in fig. 2, wherein the relationship is linear as expected.

#### Static contact angle

The wetting condition plays a significant role in micro-channels. The surface wettability is usually represented by contact angle (when an interface exists between a liquid and a solid, the angle between the surface of the liquid and the outline of the contact surface is described as the contact angle). It quantifies the wettability of a solid surface. The pseudo-potential LBM

*i. e.*  $w_d$ . The continuous phase injects into the main channel and the disperse phase flows into the two lateral channels. In the simulations, a velocity boundary conditions developed by Zou and He [38] is imposed on the three inlets. The equilibrium boundary condition [39] is used for the outlet. For all the solid walls, the half-way bounce-back boundary condition [40] is applied to achieve the non-slip boundary condition on the walls.

is an ideal method for modeling of the wetting condition, which is extremely difficult to handle using other multi-phase LBM. In pseudo-potential LBM, the different wetting condition could be specified by varying the interaction strength between the solid and two-phases,  $G_{sw}$ . In order to verify our code for determining the contact angles, 2-D simulation was carried out and was compared with 2-D results from the Huang *et al.* [35]. A semi-circular drop with radius  $R = 25$  lattice unit is initially located on the solid bottom surface. The periodic boundary condition is applied for both the east and west sides and the half-way bounce-back boundary condition is applied for both the upper and lower sides to reproduce no-slip boundary conditions. The computational domain is  $200 \times 100$  lattice units. Figure 3 shows the obtained contact angle of the present study in comparison with the numerical results of Huang *et al.* [35]. Also, value of different contact angles of present study in comparison with Huang *et al.* [35] is listed in tab. 1. The comparison indicates that the results have good agreement with numerical data.

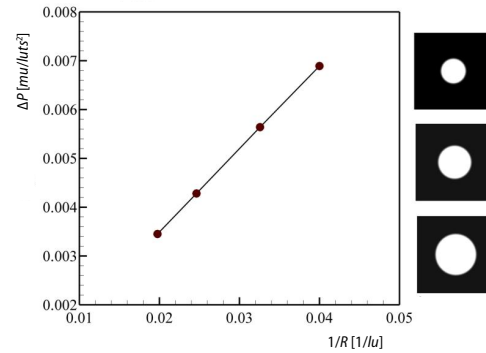


**Figure 2. Comparison simulation results with the Laplace test;  $lu$ ,  $ts$ , and  $mu$  are the length, time, and the mass scales in lattice unit**

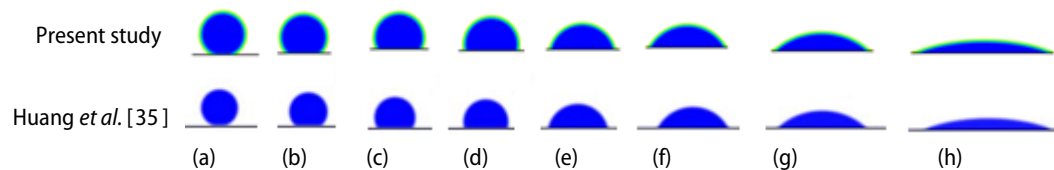


**Figure 3. Comparison between contact angles of the present study with the results of Huang *et al.* [35]**

**Table 1. Value of different contact angles of present study in comparison with Huang *et al.* [35]**

	a	b	c	d	e	f	g	h
Huang <i>et al.</i> [35]	157.5	135.7	119.5	105.4	85	62.4	43.8	21.6
Present study	158.3	135.1	117	103.2	75.3	59.5	40.6	18.9

### Drop formation in cross-junction micro-channel

The formation mechanism of drop in cross-junction is shown in fig. 4 and it is compared to the experimental results of Wu *et al.* [13] at the same condition. The experimental and present simulations are shown in the left and right sides of fig. 4. Three stages of the drop formation mechanism can be seen: expansion stage, necking stage, and final stage. Figures 4(a)-4(c) show the expansion stage where the continuous phase expands and enters the main channel. This stage takes place slowly and steadily. Figures 4(d) and 4(e) describe the necking stage that continuous phase is compressed by dispersed phase from the two sides. The tip of continuous phase kept expanding, and tail of continuous phase kept thinning. The interfacial tension forces increase here and become strong due to the sudden change in the curvature of the interface. The necking stage happens very fast. The continuous phase is suddenly cut-off from the bulk and a drop is generated. After the cut-off, the tail of the formed drop retracts to

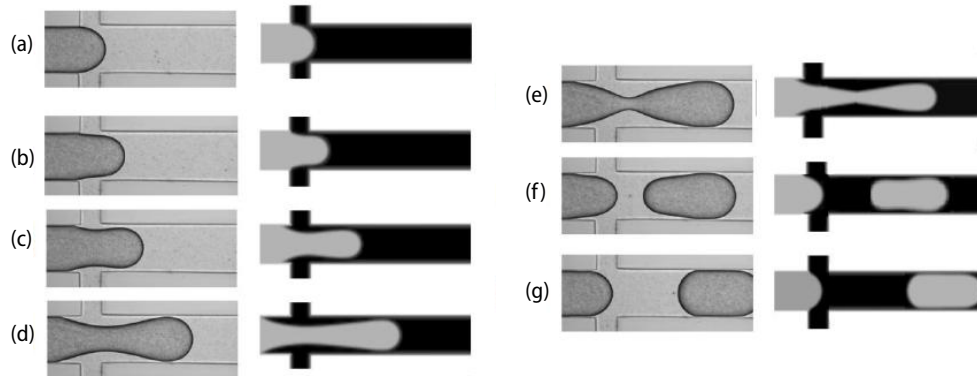


**Figure 4. Different stages of drop formation mechanism in a cross-junction micro-channel; (a)-(d) experimental result of Wu *et al.* [13], (e)-(g) present results**

the main body of drop. The recoiling of continuous phase backs into inlet channel. Figures 4(f) and 4(g) display the final stage in which the generated drop tends to minimize its surface area and attains a particular shape. This mechanism is repeated and drops that have constant shapes and sizes are regularly formed.

## Results and discussion

After validating the numerical method with previous studies, the behavior of  $f$  drop formation and the effects of flow rate ratio, capillary number and viscosity ratio on the drop formation are discussed.

### Effect of capillary number

Figure 5 shows the effect of capillary number numbers on the flow patterns at  $Q = 0.67$ ,  $\rho = 30$ ,  $\mu = 0.5$ ,  $w = 0.5$ , and  $\theta_{eq} = 150^\circ$ . It can be seen that changing capillary number yields three different regimes: jetting, drop, and slug regime: In jetting regime, fig 5(a), the surface tension is not high enough to overcome the shear force. Then, no drop is formed. In the drop regime, fig 5(b), spherical drops are regularly formed in the front of mixing section. In fact, the shear force

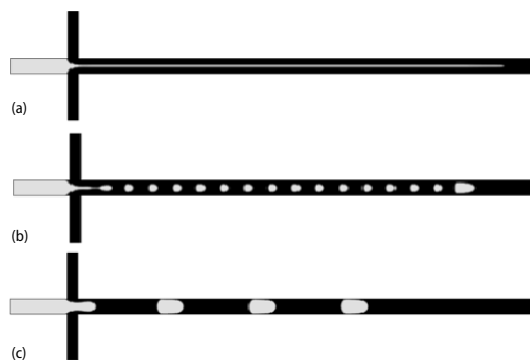


**Figure 5. Effect of capillary number on the flow patterns at  $Q = 0.67$ ,  $\rho = 30$ ,  $\mu = 0.5$ ,  $w = 0.5$ , and  $\theta_{eq} = 150^\circ$ ; (a)  $Ca = 3$ , (b)  $Ca = 0.03$ , and (c)  $Ca = 0.0015$**

is high enough to overcome surface tension. It can be observed that the drop diameter is smaller than the width of channel. Also, a regular pattern of drops is generated with a uniform radius and a fixed frequency, except the first drop which is much larger than compared to the others. In the slug regime, fig 5(c), the squeezing pressure plays a dominant role for drop breakup. The drop fills the main channel, leading to the pressure upstream of the continuous phase increases. The disperse phase squeezes the continuous phase and elongates it toward the downstream of main channels. The neck of continuous phase becomes thin enough and eventually breaks up into a drop. Also, a thin disperse film layer was always

present between the continuous and the channel wall, preventing the direct contact of the two, fig 5(c).

The pressure distribution along the central axis of the micro-channel is shown in fig. 6 at  $Ca = 0.0015$ ,  $Q = 0.67$ ,  $\rho = 30$ ,  $\mu = 0.5$ ,  $w = 0.5$ , and  $\theta_{eq} = 150^\circ$ . Pressure distribution of two-phase flow in micro-channel varies due to friction caused by viscous forces and surface tension at the interface of two-phases. Laplace pressure which represents the surface tension term in pressure distribution is indicated by a jump across the interface of the two phases. The upper lines show continuous phase while the lower ones indicate disperse phase.

#### Effect of flow rate ratio

Figure 7 shows the shape of drops generated as a function of flow rate ratio at  $Ca = 0.003$ ,  $\rho = 30$ ,  $\mu = 0.5$ ,  $w = 0.5$ , and  $\theta_{eq} = 150^\circ$ . As flow rate ratio decreases, drops length decrease, and the interval between the generated drops increase. For better discussion, the drops length rate ( $DL/w_c$ ) and the interval rate ( $DI/w_c$ ) vs. the flow rate ratio in slug regime at  $\rho = 30$ ,  $\mu = 0.5$ ,  $w = 0.5$ , and  $\theta_{eq} = 150^\circ$  are presented in figs. 8(a) and 8(b), respectively. The DL and DI denote drop length and distance between two neighboring drops, respectively. With the increasing in the flow rate, the size of the generated drops increases. The increase is approximately linear on  $Q$ , fig 8(a). Also, the interval rate decreases when the flow rate increases, fig 8(b).

#### Effect of contact angle

In order to investigate the influence of the contact angle on the final shape of drop, we changed the interaction strength between the solid and two-phases,  $G_{sw}$ , to get different contact

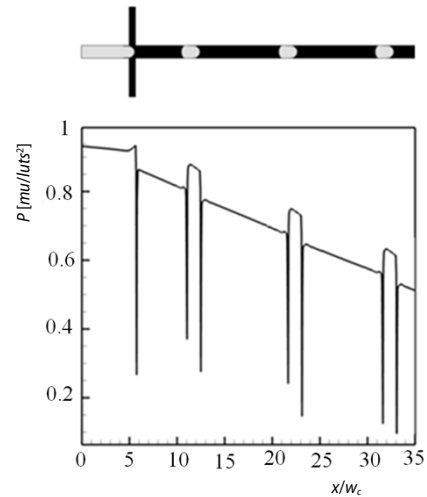


Figure 6. The pressure distribution along the central axis of the micro-channel;  $lu$ ,  $ts$ , and  $mu$  are the length, time, and the mass scales in lattice unit

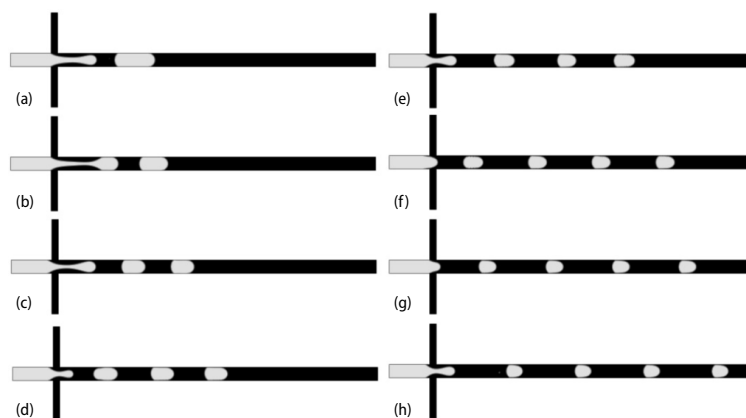


Figure 7. Effect of flow rate ratio on the shape of generated drops at  $Ca = 0.003$ ,  $\rho = 30$ ,  $\mu = 0.5$ ,  $w = 0.5$ , and  $\theta_{eq} = 150^\circ$  for different flow rate ratio; (a)  $Q = 2.0$ , (b)  $Q = 1.68$ , (c)  $Q = 1.33$ , (d)  $Q = 1.0$ , (e)  $Q = 0.8$ , (f)  $Q = 0.67$ , (g)  $Q = 0.57$ , and (h)  $Q = 0.5$

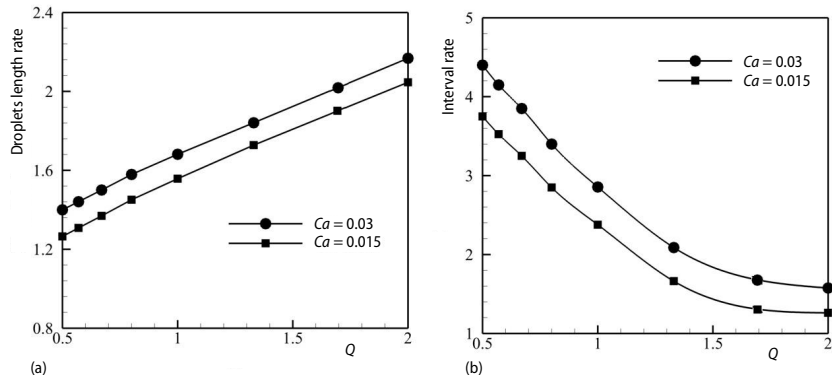


Figure 8. (a) Drop length rate vs. the flow rate ratio and (b) the interval rate vs. the flow rate ratio

angles while other parameters are not changed. Figure 9 shows the final shape of drop at four different contact angle  $\theta_{\text{eq}} = 90^\circ, 120^\circ, 150^\circ,$  and  $180^\circ$  for  $Ca = 0.003, \rho = 30, \mu = 0.5, w = 0.5,$  and  $Q = 1.33$ . With increasing contact angle, the wall rejects the continuous phase and attracts the disperse phase, and thus drops length and the interval between the generated drops increase while number of generated drops decrease.

#### Effect of viscosity ratio

The effect of viscosity ratio,  $\mu$ , is evaluated by comparing three different values of  $\mu = 0.5, 2,$  and  $4$  in fig. 10 for  $Q = 0.5, \rho = 30, w = 0.5,$  and  $\theta_{\text{eq}} = 150^\circ$  in squeezing regime  $Ca = 0.009$ . It is observed that viscosity ratio has no effect in the final shape of drop. Also, drop length and distance between drops is solely affected by viscosity ratio. It is very similar to the experimental result of Christopher *et al.* [6] in the T-junction micro-fluidic devices. They found that the length of drop is independent of viscosity ratio in squeezing regime.

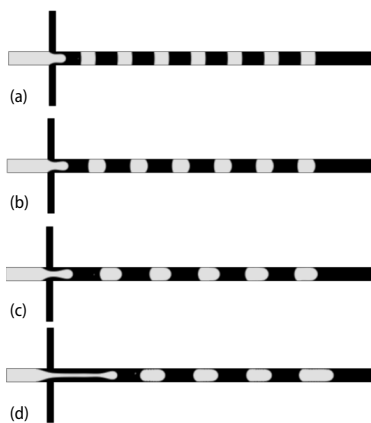


Figure 9. Effect of contact angle on the final shape of the drop for; (a)  $90^\circ,$  (b)  $120^\circ,$  (c)  $150^\circ,$  and (d)  $180^\circ$  for  $Ca = 0.003, \rho = 30, \mu = 0.5, w = 0.5,$  and  $Q = 1.33$

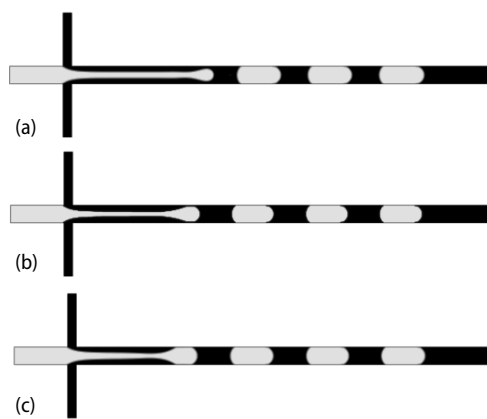


Figure 10. Effect of viscosity ratio for  $Ca = 0.002, \rho = 30, w = 0.5, Q = 1.33,$  and  $\theta_{\text{eq}} = 150^\circ;$  (a)  $\mu = 0.5,$  (b)  $\mu = 2.0,$  and (c)  $\mu = 4.0$

## Conclusion

In this study, drop formation in cross-junction micro-channel has been investigated numerically using the LBM with the pseudo-potential model. The numerical simulations were validated against numerical and experimental results. The affects of capillary number, flow rate ratio, contact angle, and viscosity ratio on the flow patterns, drop length and interval between drops is investigated and highlighted. Conclusion of the present study can be summarized as follows.

- It is found that LBM is a suitable approach for simulation of two-phases in the micro-channels.
- The drop formation process has different regimes, namely, jetting, drop and squeezing regimes.
- With increasing in the flow rate ratio in the squeezing regime, the drop length increases while the interval between drops decreases.
- The drops length and the interval between the generated drops increase as the contact angle increases.
- The drop length and distance between drops is solely affected by viscosity ratio.

## Nomenclature

Bo – Bond number, ( $= \rho_c g w_c^2 / \sigma$ ), [-]

C – lattice speed

Ca – capillary number, ( $= \mu_c U_c / \sigma$ )

$c_s$  – speed of sound

DL – droplet length,

DI – interval between droplets

e – microscopic velocity

F – external force

f – distribution function for flow field

$f^{eq}$  – equilibrium distributions function

g – gravity

$G_{\sigma\bar{\sigma}}$  – interaction strength between two components  $\sigma$  and  $\bar{\sigma}$

$G_{\sigma w}$  – interaction strength between solid and fluid component  $\sigma$

**u** – velocity in lattice unit

**u'** – effective velocity

$P_c$  – critical pressure,

Q – flow rate ratio ( $= U_c w_c / U_d w_d$ )

$T_c$  – critical temperature

w – width ratio,

w – weight factor

### Greek symbols

$\rho$  – density ratio

$\sigma$  – interfacial tension between phases

$\mu$  – viscosity

$\psi$  – interparticle potential

$\tau$  – relaxation time

$\delta t$  – time step size

$\omega$  – acentric factor

### Subscripts

$\sigma$  – component

c – continuous phases

d – dispersed phases

f – fluid

s – solid

## References

- [1] He, M., *et al.*, Selective Encapsulation of Single Cells and Subcellular Organelles into Picoliter and Femtoliter-Volume Droplets, *Anal. Chem.*, 77 (2005), 6, pp. 1539-1544
- [2] Chambers, R. D., *et al.*, Elemental Fluorine – Part 13. Gas-Liquid Thin Film Microreactors for Selective Direct Fluorination, *Lab on a Chip*, 1 (2001), 2, pp. 132-137
- [3] Griffiths, A. D., Tawfik, D. S., Miniaturising the Laboratory in Emulsion Droplets, *Trends Biotechnol.*, 24 (2006), 9, pp. 395-402
- [4] Kobayashi, J., *et al.*, A Microfluidic Device for Conducting Gas-Liquid-Solid Hydrogenation Reactions, *Science*, 304 (2004), May, pp. 1305-1308
- [5] Thorsen, T., *et al.*, Dynamic Pattern Formation in a Vesicle-Generating Microfluidic Device, *Phys Rev Lett.*, 86 (2001), 18, pp. 4163-4166
- [6] Christopher, G. F., *et al.*, Experimental Observations of the Squeezing-to-Dripping Transition in T-Shaped Microfluidic Junctions, *Phys Rev E.*, 78 (2008), 3, 36317

- [7] Sivasamy, J., et al., An Investigation on the Mechanism of Droplet Formation in a Microfluidic T-Junction, *Microfluidics and Nanofluidics*, 11 (2011), 1, pp 1-10
- [8] Qian, D., Lawal, A., Numerical Study on Gas and Liquid Slugs for Taylor Flow in a T-Junction Micro-Channel, *Chemical Engineering Science*, 61 (2006), 23, pp. 7609-7625
- [9] Shi, Y., Lattice Boltzmann Simulation of Droplet Formation and Flow Focusing Devices, *Computers and Fluids*, 90 (2014), Feb., pp. 155-163
- [10] Tice, J. D., et al., Formation of Droplets and Mixing in Multiphase Microfluidics at Low Values of the Reynolds and the Capillary Numbers, *Langmuir*, 19 (2003), 22, pp. 9127-9133
- [11] Kim, K. C., et al., Simultaneous Measurement of Internal and External Flow Fields around the Droplet Formation in a Microchannel, *Proceedings*, 4<sup>th</sup> KSV Conf., Seoul, Korea, 2004, pp. 80-83
- [12] Cubaud, Th., et al., Two-Phase Flow in Microchannels with Surface Modifications, *Fluid Dynamics Research*, 38 (2006), 11, pp. 772-786
- [13] Wu, L., et al., Three-Dimensional Lattice Boltzmann Simulations of Droplet Formation in a Cross-Junction Microchannel, *International Journal of Multiphase Flow*, 34 (2008), 9, pp. 852-864
- [14] Fu, T., et al., Breakup Dynamics of Slender Formation in Shear-Thinning Fluids in Flow-focusing Devices, *Chemical Engineering Science*, 144 (2016), Apr., pp. 75-86
- [15] Yue, J., et al., An Experimental Investigation of Gas-Liquid Two-Phase Flow in Single Microchannel Contactors, *Chemical Engineering Science*, 63 (2008), 16, pp. 4189-4202
- [16] Chaoqun, Y., et al., Characteristics of Slug Flow with Inertial Effects in a Rectangular Microchannel, *Chemical Engineering Science*, 95 (2013), May, pp. 246-256
- [17] Carrol, B., Hidrovo, C., Experimental Investigation of Inertial Mixing in Colliding Droplets, *Heat Transfer Engineering*, 34 (2013), 2-3, pp. 120-130
- [18] Gupta, A., Kumar, R., Lattice Boltzmann Simulation to Study Multiple Bubble Dynamics, *Int J Heat Mass Transf.*, 51 (2008), 5, pp. 5192-5203
- [19] Sajjadi, H., Kefayati, R., Lattice Boltzmann Simulation of Turbulent Natural Convection in Tall Enclosures, *Thermal Science*, 19 (2015), 1, pp. 155-166.
- [20] Fallah, K., et al., Simulation of Natural Convection Heat Transfer Using Nanofluid in a Concentric Annulus, *Thermal Science*, 21 (2017), 3, pp. 1275-1286
- [21] Alinejad, J., Fallah, K., Taguchi Optimization Approach for Three-Dimensional Nanofluid Natural Convection in a Transformable Enclosure, *Journal of Thermophysics and Heat Transfer*, 31 (2017), 1, pp. 211-217
- [22] Fallah, K., et al., Multiple-Relaxation-Time Lattice Boltzmann Simulation of Non-Newtonian Flows Past a Rotating Circular Cylinder, *Journal of Non-Newtonian Fluid Mechanics*, 177-178 (2012), June, pp. 1-14
- [23] Wang, Y.-L., Shao, X.-M., Study on Flow of Power-Law Fluid through an Infinite Array of Circular Cylinders with Immersed Boundary-Lattice Boltzmann Method, *Thermal Science*, 16 (2012), 5, pp. 1451-1455
- [24] Fallah, K., et al., Numerical Simulation of Planar Shear Flow Passing a Rotating Cylinder at Low Reynolds Numbers, *Acta Mechanica*, 223 (2012), 2, pp. 221-236
- [25] Inamuro, T., et al., A Lattice Boltzmann Method for Incompressible Two-Phase Flows with Large Density Differences, *Journal of Computational Physics*, 198 (2004), 2, pp. 628-644
- [26] Swift, M. R., et al., Lattice Boltzmann Simulation of Nonideal Fluids, *Phys. Rev. Lett.*, 75 (1995), July, pp. 830-833
- [27] Swift, E., et al., Lattice Boltzmann Simulations of Liquid-Gas and Binary Fluid Systems, *Phys. Rev. E*, 54 (1996), Nov., pp. 5041-5052
- [28] He, X., et al., Discrete Boltzmann Equation Model for Nonideal Gases, *Phys. Rev. E*, 57 (1998), 1, R13
- [29] He, X., et al., A Lattice Boltzmann Scheme for Incompressible Multiphase Flow and Its Application in Simulation of Rayleigh-Taylor Instability, *J. Comput. Phys.*, 152 (1999), 2, pp. 642-663
- [30] Shan, X., Chen, H., Lattice Boltzmann Model for Simulating Flows with Multiple Phases and Components, *Phys. Rev. E*, 47 (1993), Mar., pp. 1815-1819
- [31] Shan, X., Doolen, G., Multicomponent Lattice-Boltzmann Model with Interparticle Interaction, *J. Stat. Phys.*, 81 (1995), 1-2, pp. 379-393
- [32] Luo, L. S., Unified Theory of Lattice Boltzmann Models for Nonideal Gases, *Phys. Rev. Lett.*, 81 (1998), Aug., pp. 1618-1621
- [33] Luo, L. S., Some Recent Results on Discrete Velocity Models and Ramifications for Lattice Boltzmann Equation, *Comput. Phys. Commun.*, 129 (2000), 1-3, pp. 63-74
- [34] Bao, J., Schaefer, L., Lattice Boltzmann Equation Model for Multi-component Multi-phase Flow with High Density Ratios, *Applied Mathematical Modelling*, 37 (2013), 4, pp. 1860-1871

- [35] Huang, H., *et al.*, Proposed Approximation for Contact Angles in Shan-and-Chen-Type Multicomponent Multiphase Lattice Boltzmann Models. *Phys. Rev. E.*, 76, (2007), Dec., 066701
- [36] Shan, X., Chen, H., Simulation of Nonideal Gases and Liquid-gas Phase Transitions by the Lattice Boltzmann Equation, *Phys. Rev. E.*, 49 (1994), 4, 2941
- [37] Yuan, P., Schaefer, L., Equations of State in a Lattice Boltzmann Model, *Phys. Fluids*, 18 (2006), 4, 042101
- [38] Zou, Q., He, X., On Pressure and Velocity Boundary Conditions for the Lattice Boltzmann BGK Model, *Phys. Fluids*, 9 (1997), 6, 1591
- [39] Izquierdo, S., *et al.*, Analysis of Open Boundary Effects in Unsteady Lattice Boltzmann Simulations, *Computers and Mathematics with Applications*, 58 (2009), 5, pp. 914-921
- [40] Succi, S., *The Lattice Boltzmann Equation for Fluid Mechanics and Beyond*. Oxford-Clarendon, Oxford, UK, 2001